Magnesium hydride induced hydrogen therapy for enhanced sonodynamic therapy

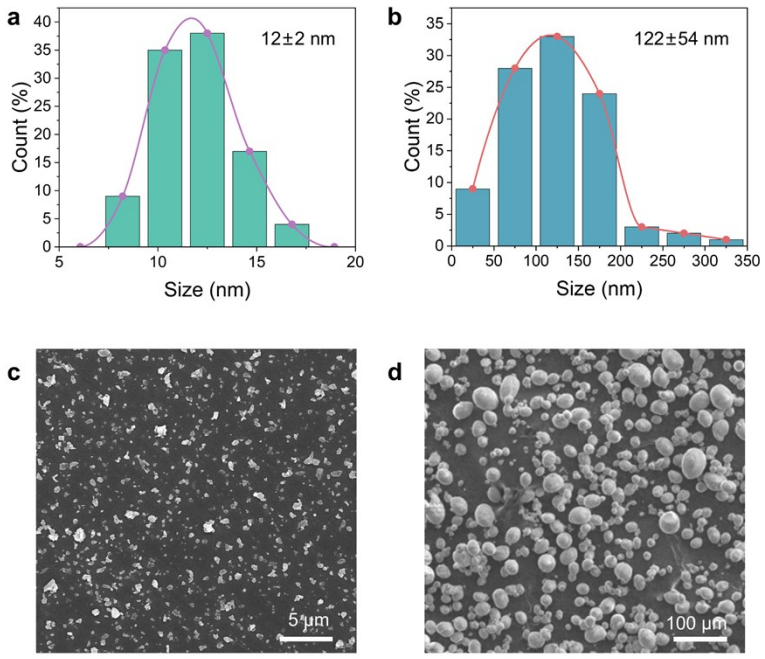

Figure S1. Particle-size distribution of (a) BTO nanoparticles and (b) MgH_2 particles. The SEM images of (c) MgH_2 nanoparticles and (d) MgH_2 powders.

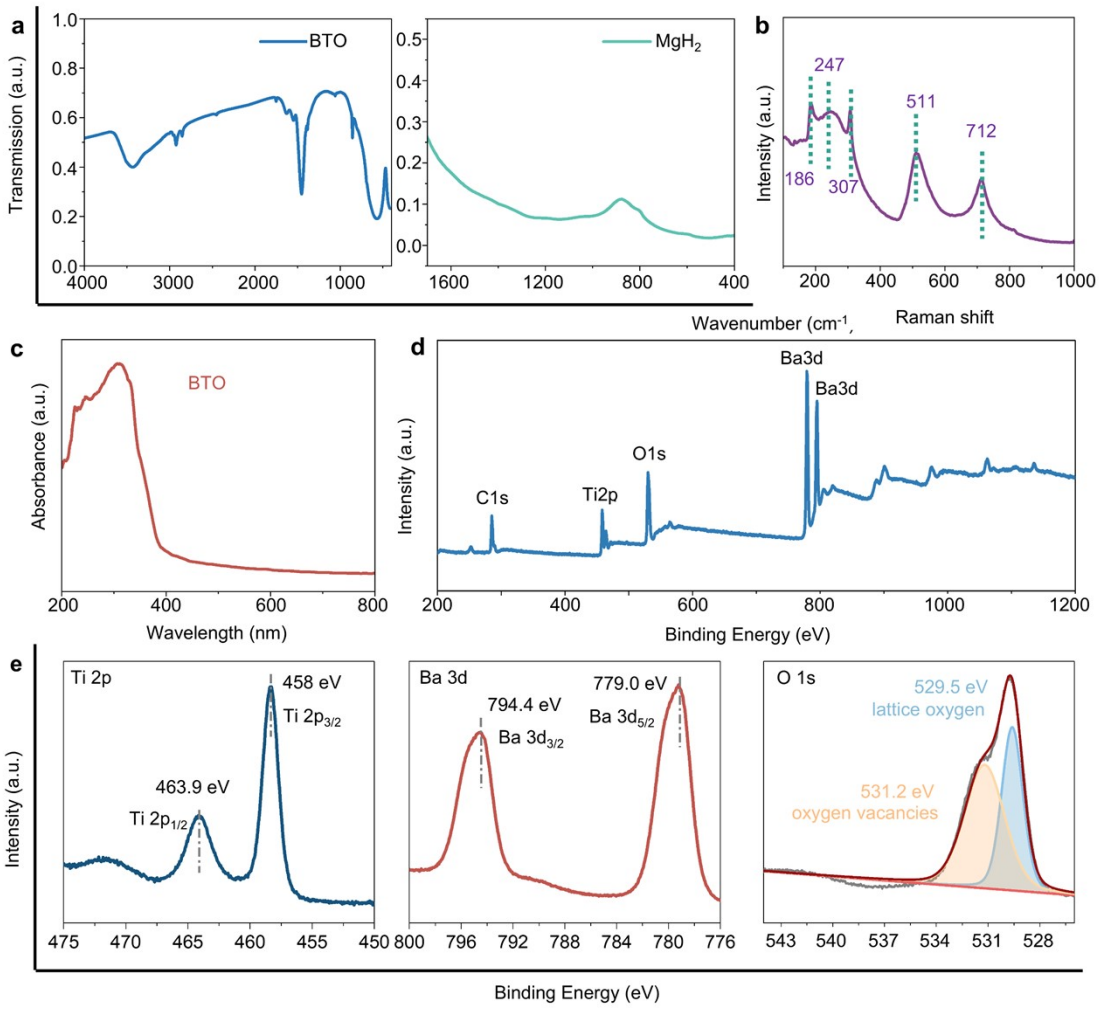

Figure S2. FITR of (a) BTO nanoparticles and MgH_2 microparticles. (b) Raman spectra of BTO nanoparticles. (c) UV-vis absorption spectrum of BTO nanoparticles. XPS spectra of (d) BTO nanoparticles and (e) Ba 3d, Ti 2p, Pd 3d, and O 1s.

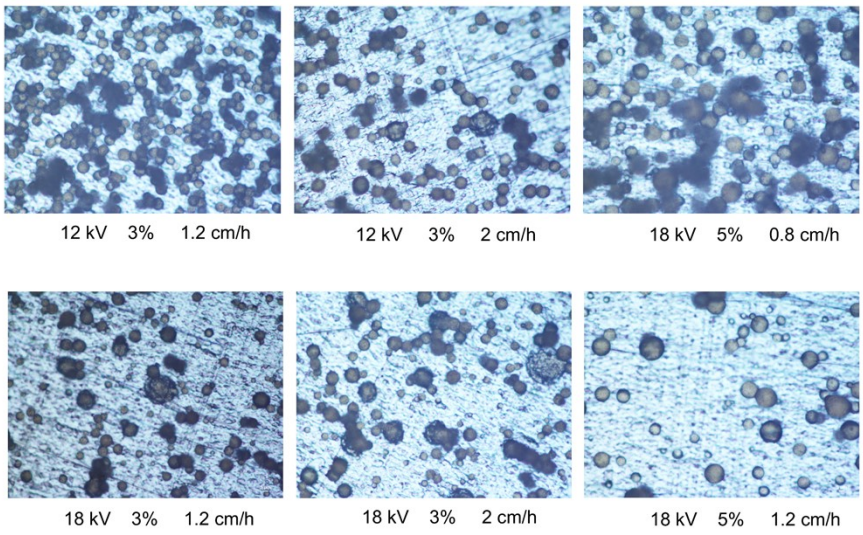

Figure S3. The photograph of MgH_2 microspheres under different parameters of electrospraying.

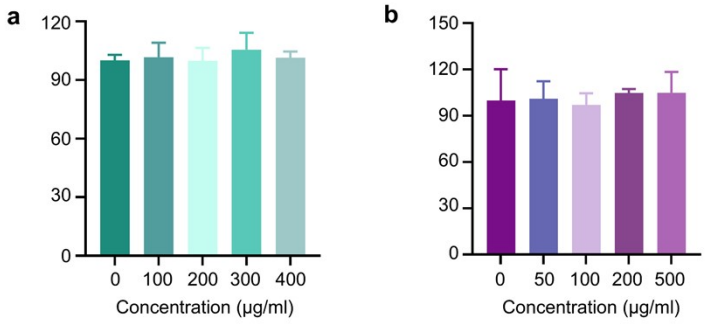

Figure S4. Relative viability of Hacat cells after incubation with various concentrations of (a) MgH_2 particles and (b) BTO nanoparticles.

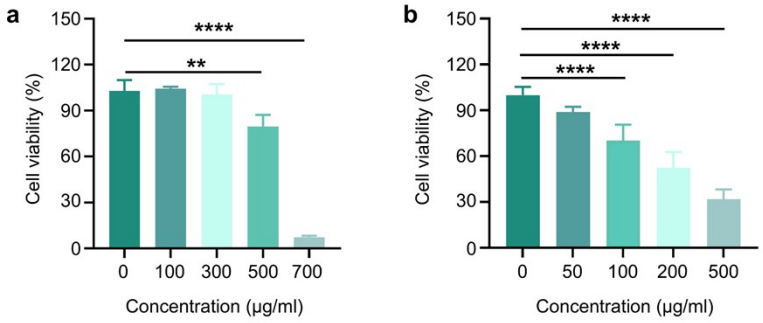

Figure S5. Relative viabilities of B16F10 cells after incubation with various concentrations of (a) MgH_2 particles and (b) BTO nanoparticles under US irradiation.

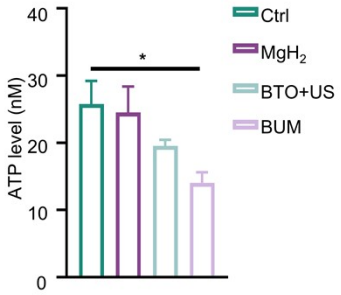

Figure S6. The intracellular ATP levels of B16F10 cells after different treatments. *P < 0.05, **P < 0.01, ***P < 0.001.

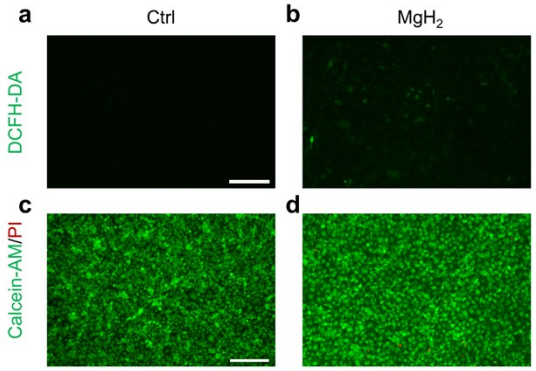

Figure S7. (a-b) The levels of ROS in B16F10 cells after different treatments were detected by DCFH-DA staining (scale bar = 200 μm). (c-d) Calcein-AM/PI fluorescence images of B16F10 cells after different treatments. Live cells (green) and dead cells (red) were detected by Calcein-AM/PI staining, respectively (scale bar = 200 μm).

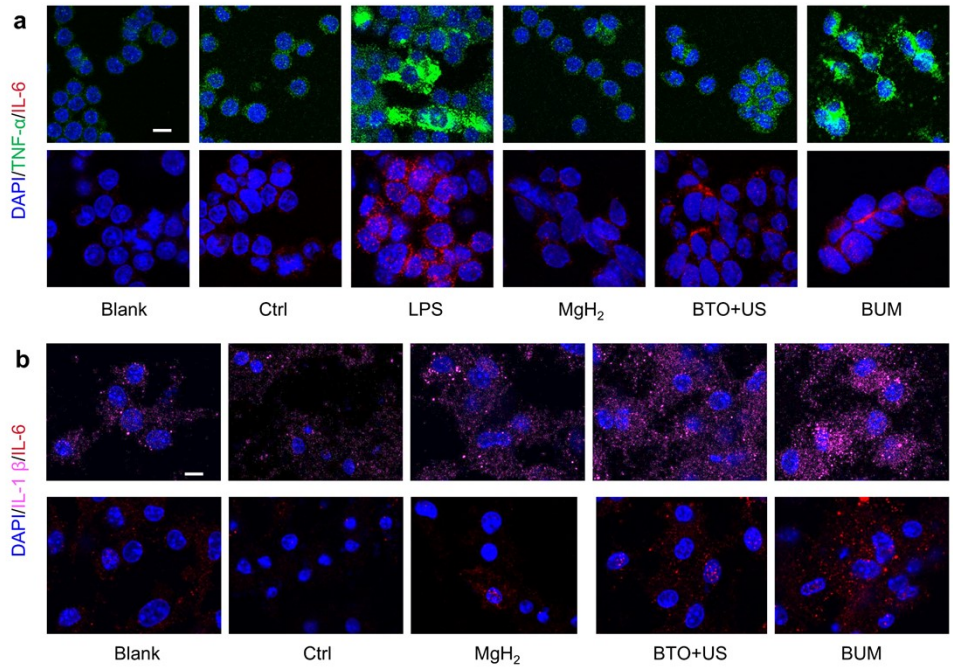

Figure S8. CLSM images of (a) RAW 264.7 cells and (b) primary macrophages (scale bar = 10 μm).

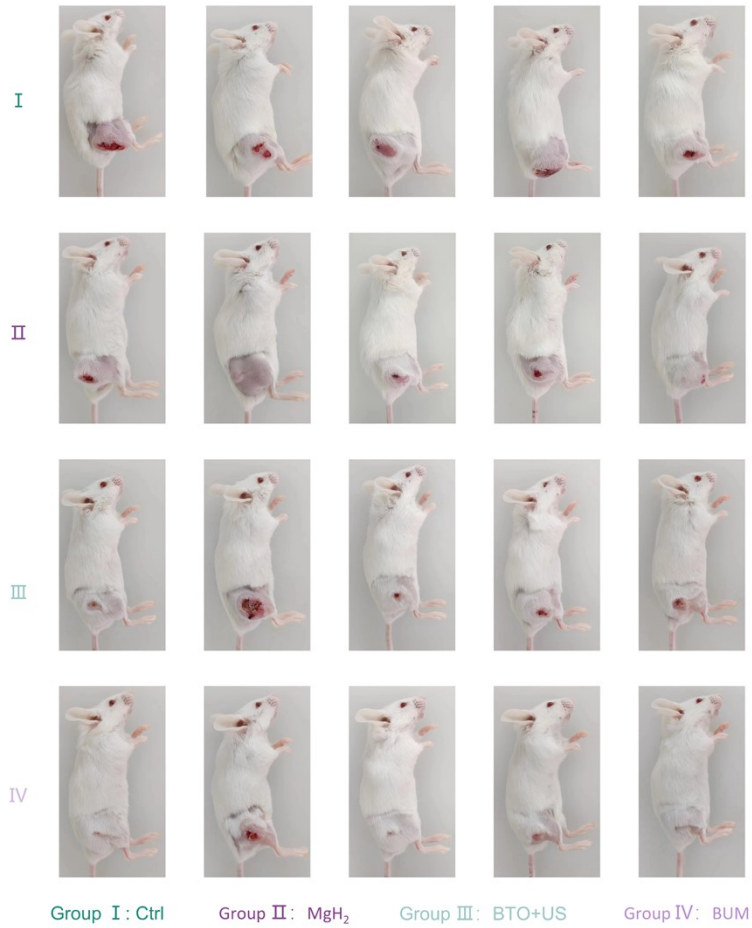

Figure S9. The photograph of CT26 tumor-bearing mice after different treatments (n=5).

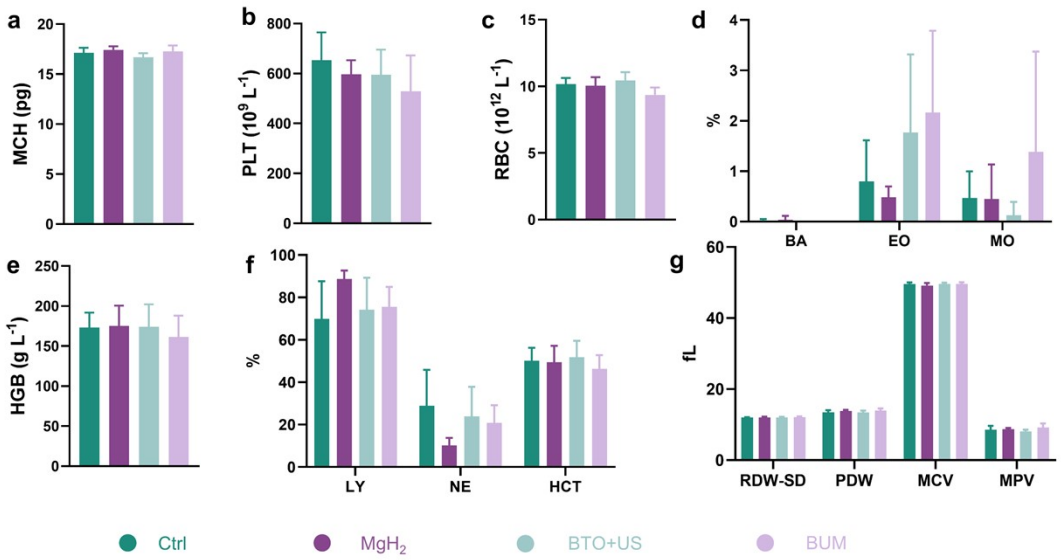

Figure S10. The blood routine indexes analysis (including mean corpuscular hemoglobin [MCH], platelets [PLT], red blood cells [RBC], basophil [BA], eosinophilic granulocyte [EO], monocyte [MO], hemoglobin [HGB], lymphocyte [LY], neutrophilic granulocyte [NE], hematocrit [HCT], standard deviation of red blood cell distribution width [RDW-SD], platelet distribution width [PDW], mean corpuscular volume [MCV] and mean platelet volume [MPV]) of the mice after different treatments.

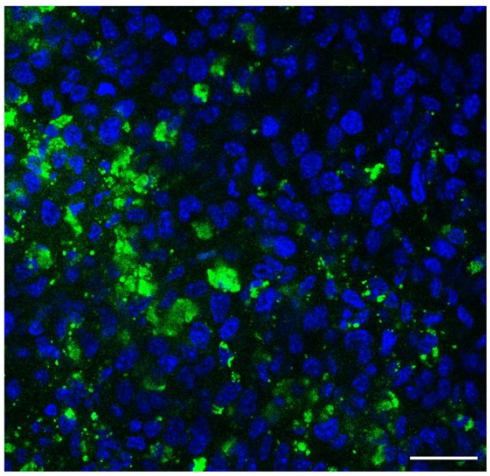

Figure S11. The fluorescence imaging demonstrates the tumor distribution profile of FITC-conjugated BTO nanoparticles (scale bar=25 μm).

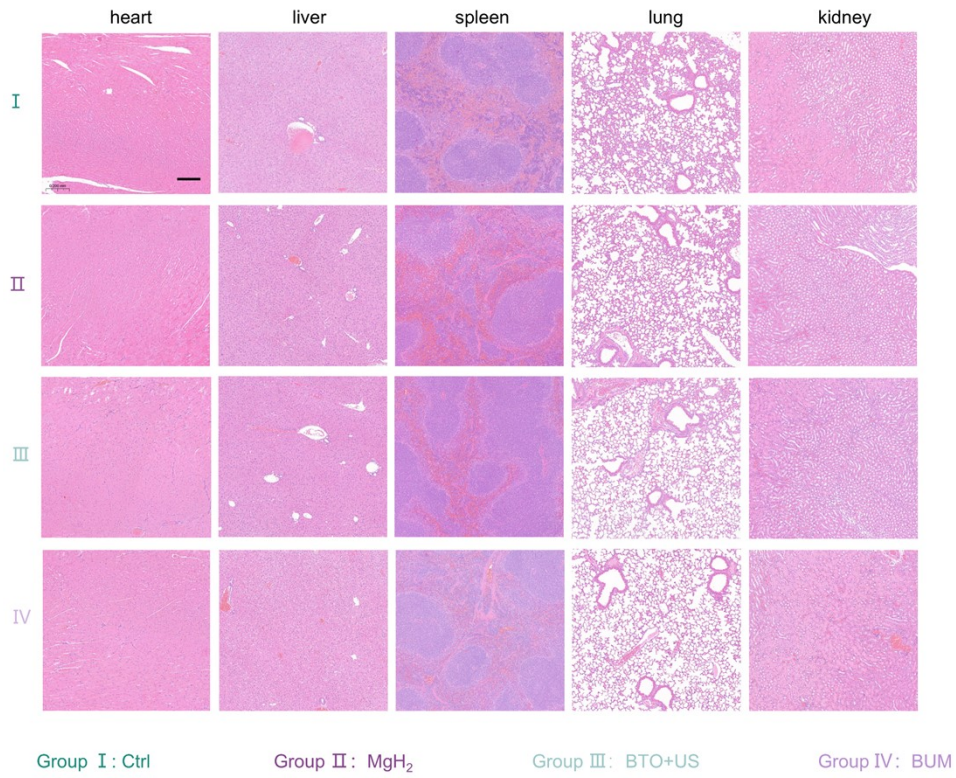

Figure S12. H&E staining of the major organs of the mice after different treatments (scale bar= 200 μm).

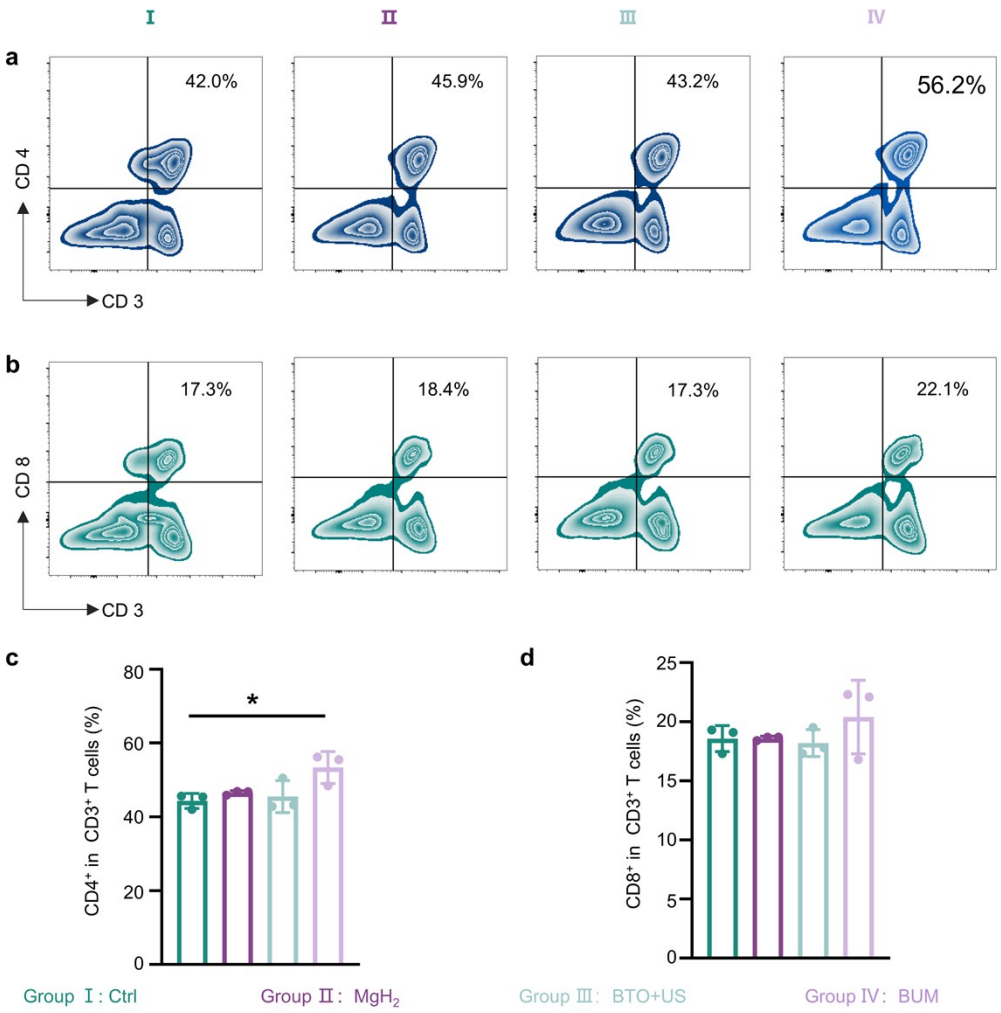

Figure S13. (a) The flow cytometric analysis results and (c) quantification results of $CD4^+$ T cells ($CD45^+CD3^+CD4$ within the lymph node after different treatments (n=3). (b) The flow cytometric analysis results and (d) quantification results of $CD8^+$ T cells ($CD45^+CD3^+CD8^+$) within the lymph node after different treatments (n=3).

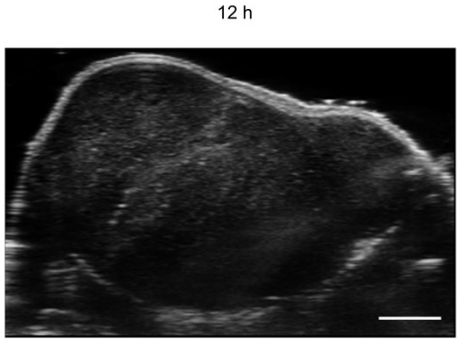

Figure S14. Ultrasonic imaging of CT26 tumor-bearing mice after injection of PEG 200 for 12 h only (scale bar = 3 mm).

Experimental section

Murine immune cell subset characterization in vivo

Treg cells: CD45-PE-Cy7, CD3-perCP-Cy5.5, CD4-APC, Foxp3-PE, T cells: CD45-PE-Cy7, CD3-perCP-Cy5.5, CD4-APC, CD8-FITC, M1 macrophages: CD45-PE-Cy7, CD11b-BV650, F4/80-BV510, CD80-FITC, M2 macrophages: CD45-PE-Cy7, CD11b-BV650, F4/80-BV510, CD206-APC, PD-1 expression: CD45-PE-Cy7, CD3-perCP-Cy5.5, aPD-1-PE.